coatings

MDPI

Article

Surface Modification of Bacterial Cellulose by Copper and Zinc Oxide Sputter Coating for UV-Resistance/Antistatic/Antibacterial Characteristics

Muhammad Wasim, Muhammad Rafique Khan, Muhammad Mushtaq, Awais Naeem, Mengchen Han and Qufu Wei *

Key Laboratory of Eco Textiles, Jiangnan University, Wuxi 212242, Jiangsu, China; Muhammad_wasim786@yahoo.com (M.W.); khan_ju@hotmail.com (M.R.K.); mmushtaq63@hotmail.com (M.M.); mawaisnaeem@hotmail.com (A.N.); 15061885905@163.com (M.H.)

* Correspondence: qfwei@jiangnan.edu.cn

Received: 3 March 2020; Accepted: 4 April 2020; Published: 7 April 2020

Abstract: In our study, the surface of bacterial cellulose was successively modified by copper and zinc oxide nanoparticles using direct current (DC) magnetron sputtering and radio frequency (RF) reactive sputter coating techniques. The target materials, copper and zinc, were 99.99% pure and used in the presence of argon (Ar) gas, while zinc nanoparticles were sputtered in the presence of oxygen gas to make zinc oxide nanoparticles. The as-prepared bacterial cellulose/copper/zinc oxide nanocomposite has good ultraviolet resistance, anti-static and antibacterial characteristics. The surface morphology and chemical composition of the nanocomposite were examined by X-ray photoelectron spectroscopy (XPS), X-ray diffraction (XRD) and energy-dispersive X-ray spectroscopic (EDS) techniques. The prepared bacterial cellulose/copper/zinc oxide nanocomposite illustrates excellent ultraviolet resistance (T.UVA%; 0.16 ± 0.02, T.UVB%; 0.07 ± 0.01, ultraviolet protection factor (UPF); 1850.33 ± 2.12), antistatic behavior (S.H.P; 51.50 ± 4.10, I.E. V; 349.33 ± 6.02) and antibacterial behavior (Escherichia coli; 98.45%, Staphylococcus aureus; 98.11%). Our nanocomposite prepared by sputter coating method could be a promising and effective candidate for ultraviolet resistance, antistatic and antibacterial in term of functional, technical, medical and in many daily life applications.

Keywords: bacterial cellulose; sputter coating; ultraviolet resistance; anti-static; antibacterial; copper; zinc oxide

1. Introduction

In the modern age, metallic semiconductor nanocomposites are studied extensively due to their high potential for applicability in daily life [1–5]. Such types of nanocomposites are enriched with mechanical, physical and chemical characteristics, which enhance their applications in sensitive sensors, pharmaceutical, medical, optical, electronic gadgets and devices. Copper and zinc oxide nanoparticles are used abundantly for the formation of nanocomposites with polymers and cellulosic materials; copper has excellent electrical, optical and chemical properties, whereas zinc oxide possesses high binding energy, performs efficient photocatalysis, and has excellent thermal properties. These types of metals and metals oxide are eco-friendly, on top of being low cost with non-toxic behavior and easily available commercially [6–14].

Copper nanoparticles have good antibacterial and thermal characteristics; in addition, their metallic ions can restrict the activities of proteins clusters and improve the surface of the film. Additionally, because of their biodegradability and high stability, they are suitable to be used with cellulosic materials [15]. In industrial applications, a requirement of many cost-effective instruments is to control microwaves, thereby absorbing harmful radiation. Copper has gained

extensive attention toward its use as a conductive material due to its low resistance characteristic in such applications. Cellulosic materials such as bacterial cellulose (BC) do not show any type of bactericidal property [16]. In order to acquire the bactericidal characteristic from bacterial cellulose, many scientists have worked on bacterial cellulose, that work encompassing several types of metals and metal oxide nanoparticles, among which Cu, CuO and ZnO conclusively exist [17,18]. Additionally, Zinc oxide has distinguished properties and has been considered for serval applications in terms of piezoelectric gadgets, semiconductors and sensors, and for antimicrobial functions [19,20]. Nowadays, researchers have more interest in using zinc oxide in the composition of nanoparticles with different approaches to regulate its structure and scope. Preparation of a nanocomposite with suitable base materials and zinc oxide nanoparticles could advance multifunctional materials, which exhibit a wide range of UV-resistance and antibacterial applications [21,22].

Human beings, as well as other living organisms, are affected by ultraviolet radiation in this universe. A decrease in environmental pollution has gained more attention, but there still needs to be a type of composite which can resist ultraviolet radiation to save the lives of all creatures [23,24]. The main cause of skin cancer is ultraviolet radiation, which is a medium of free radicals. Moreover, it is a cause of environmental degradation; and damages various pigments and materials and degrades their physical characteristics [25]. The deposition of zinc oxide nanoparticles on substrates is an excellent opportunity not only for antimicrobial characteristics but for ultraviolet radiation protection too [26]. The application of zinc oxide with other materials provides long term stability against ultraviolet radiation and improves the absorption capacity of its base material [27,28]. Besides, zinc oxide nanoparticles' restriction capacity against ultraviolet radiations depends upon the morphological structure and size of nanoparticles [29]. Zinc oxide is a common element in many sunscreens, which converts ultraviolet radiation to infrared, yet infrared could be dangerous depending on the exposure [30].

The application of a zinc oxide nanocomposite has been studied extensively in terms of optical, electrical, optoelectronic and photochemical characteristics. The high energy surface area of zinc oxide nanocomposites presents excellent characteristics in the applications of sensing devices, color creation and antimicrobial materials [31–34].

The fabrication of metallic and metallic oxide nanoparticles on polymers and cellulosic materials has been reported with several methods and techniques, among which are hydrothermal, sol–gel, chemical deposition, photoreduction and laser deposition methods, according to applications [35–39]. Meanwhile, high temperatures, high pressures, costly machines, harmful elements and high process times are those factors which limit the material applications. Thus, to avoid these types of problems, a unique and fast method for the formation of a nanocomposite material is a magnetron sputter coating, which can be economically and commercially fit. The method of reactive sputter coating of ZnO nanoparticles improves the UV radiation absorbency [40]. The features of this method describe its characteristics in terms of smooth deposition of nanoparticles; high crystalline formation; preparation of conductive materials; and optical and magnetic film preparation [41–43].

Bacterial cellulose is a three-dimensional nanofibrils structure prepared by *Acetobacter xylinum* [44]. It possesses outstanding characteristics—biocompatibility, high porosity, crystallinity (63–71%), good tensile strength and increased water holding capacity [45]. Additionally, in recent years BC has gained more attention due to its excellent mechanical and physical properties as a novel substrate for porous aerogel nanocomposites [46–48]. The pellicles of bacterial cellulose play a major role in the medical field in terms of wound dressing, because of the protection from infection they grant, and their being suitable for drug delivery. The recent development of BC for burned wound dressing is Albeit BC, which works efficiently against bacterial infections [49].

Several studies have been done recently on bacterial cellulose, including sputter coating of copper with other metals in which copper may oxidize, and these nanocomposites are used for different purposes [50]. In specific, those studies were mainly on the compatibility of deposited nanoparticles'

characteristics for the development of printed circuit boards, electromagnetic interference (EMI) shielding, etc.

However, in our study, the copper/zinc oxide nanocomposite, apart from ultraviolet resistance characteristics, also possesses antimicrobial, antistatic and anti-oxidation characteristics, which enhance its applications in different areas according to the requirements. Moreover, copper oxidizes in an open environment; therefore, to protect it from oxidation, a zinc oxide layer was deposited on the surface of bacterial cellulose/copper. In addition, the deposition of the zinc oxide layer enhances the characteristics required of the nanocomposite.

This work deals with the surface modification of bacterial cellulose by sputter coating of copper and zinc oxide nanoparticles to make bacterial cellulose/copper/zinc oxide nanocomposite. The chemical composition and morphological structure were examined through X-ray photoelectron spectroscopy (XPS), energy dispersive X-ray spectroscopic (EDS) and X-ray diffraction (XRD) techniques. Additionally, the antibacterial characteristics of copper and zinc oxide were studied by the *Escherichia coli* and *Staphylococcus aureus* quantitative bacterial growth method. Similarly, UV-resistance and antistatic properties were studied by ultraviolet transmittance analyzer and statistic honest meter, respectively. So our study revealed that the deposition of copper and zinc oxide nanoparticles on bacterial cellulose by the magnetron sputter coating technique makes an excellent nanocomposite candidate for UV-resistance/antistatic/antibacterial characteristics.

2. Experimental Methods

2.1. Materials

The high purity (99.99%) targets copper and zinc were purchased from C.M. Technology Pvt., Ltd.(Shanghai, China). Meanwhile, glucose, mannitol, bacto-peptone and sodium hydro-oxide were used to produce the bacterial cellulose (BC) in the in-house laboratory of Jiangnan University, Wuxi, China. Similarly, the materials for the antibacterial test were soya peptone, tryptone, yeast extract and agar from S.C. Reagent Pvt., Ltd. (Shanghai, China). Sodium chloride, potassium chloride, dipotassium hydrogen phosphate and trihydrate sodium phosphate dibasic anhydrous were purchased from SCR Pvt., Ltd. (Shanghai, China). All solutions were prepared with distilled water. Chemicals were graded analytically in the in-house laboratory of Jiangnan University, Wuxi, China.

2.2. Synthesis of Bacterial Cellulose

The bacterial cellulose (BC) was prepared by a static incubation growth method of *Gxylinus acetobacter* with (0.6% glucose, 0.8% bacto-peptone, 2.5% yeast) Hestrin and Schramm (HS) medium dissolved in distilled water. The process was performed at 30 °C for 6–7 days to get final pellicles of bacterial cellulose. Then BC pellicles were rinsed with 0.1 M sodium hydroxide (NaOH) at 80 °C for 4 h to get a clearer form of BC. Finally, all BC pellicles were rinsed with distilled water [51].

The solution which was prepared for the synthesis of BC was transparent orange on the first day, but with the passage of time, it became turbid. The gradual formation of the BC membrane was displayed by the sixth day. It was a white gel form of bacterial cellulose pellicles [52]. The bubble formation over the surface of the flask illustrated the fibrous structure of the bacterial cellulose that gradually became tightly interlinked in the culture [53]. The formation of bacterial cellulose became slow due to the reduction of oxygen. Then, a new layer of BC fibrils started on the same bacterial cellulose pellicles, eventually reaching the uniform and compact structure presented in Figure 1A,B.

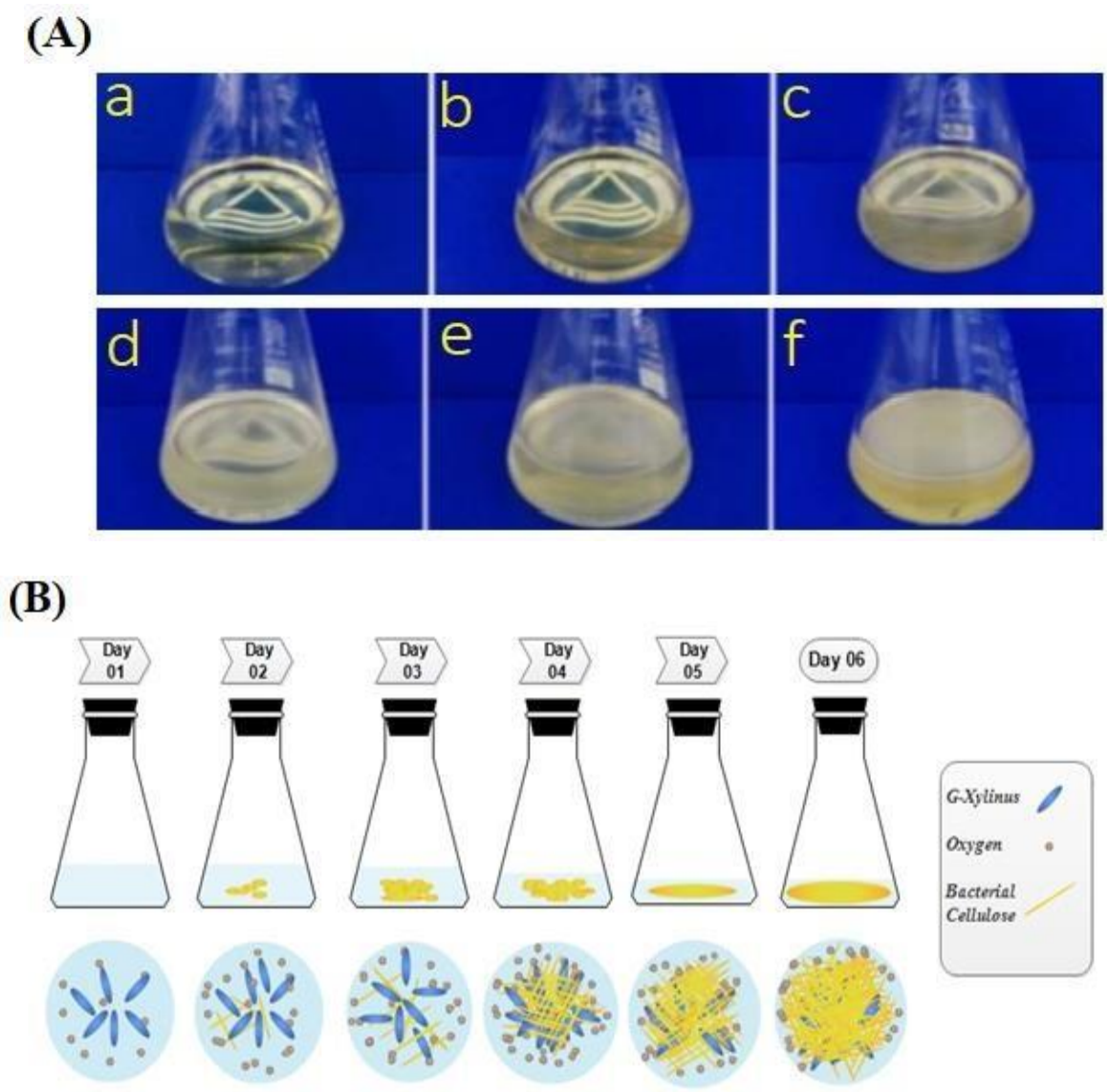

Figure 1. The synthesis of pure bacterial cellulose: (**A**) photographic presentation of six days (a: 1, b: 2, c: 3, d: 4, e: 5, f: 6) of bacterial cellulose cultivation; (**B**) schematic representation of pure bacterial cellulose cultivation in order to follow days 1–6.

2.3. Synthesis of Copper and Zinc Oxide Nanocomposite Films

The surface bacterial cellulose was functionalized by copper and zinc oxide nanoparticles with the help of DC and RF magnetron sputter coating (JPG-450) methods, as shown in Figure 2. The procedure for deposition of nanoparticles on the bacterial cellulose surface was as followed: A high purity (99.99%) target of copper was fixed on the cathode end by 80 mm distance of the surface of the bacterial cellulose. The pressure of Ar (purity; 99.99%) gas was kept 8.0×10^{-4} Pa in the chamber. The Ar gas was stabilized at 20 sccm by panel control. The substrate moving speed was set to 90 rpm to achieve smooth deposition of copper nanoparticles on the bacterial cellulose by DC magnetron sputter coating, and the coating time was set 60 min with 50 W. Similarly, a pure (99.99%) zinc target was placed to get the zinc oxide nanoparticle layer on BC/Cu substrate by the RF magnetron sputter coating method. The vessel was vacuumed before sputtering by insertion of gas, and the pressure was fixed at 1.0 Pa. The flows of Ar and oxygen were kept to 55 sccm and 5 sccm respectively, with a 100 W power supply to carry out the sputtering process. The coating time was set to 30 min. The coating in both (DC, RF) processes was done on only one side of bacterial cellulose. After sputter coating,

the final nanocomposite of bacterial cellulose, copper and zinc oxide was taken out from the chamber to measure its physical and chemical characteristics.

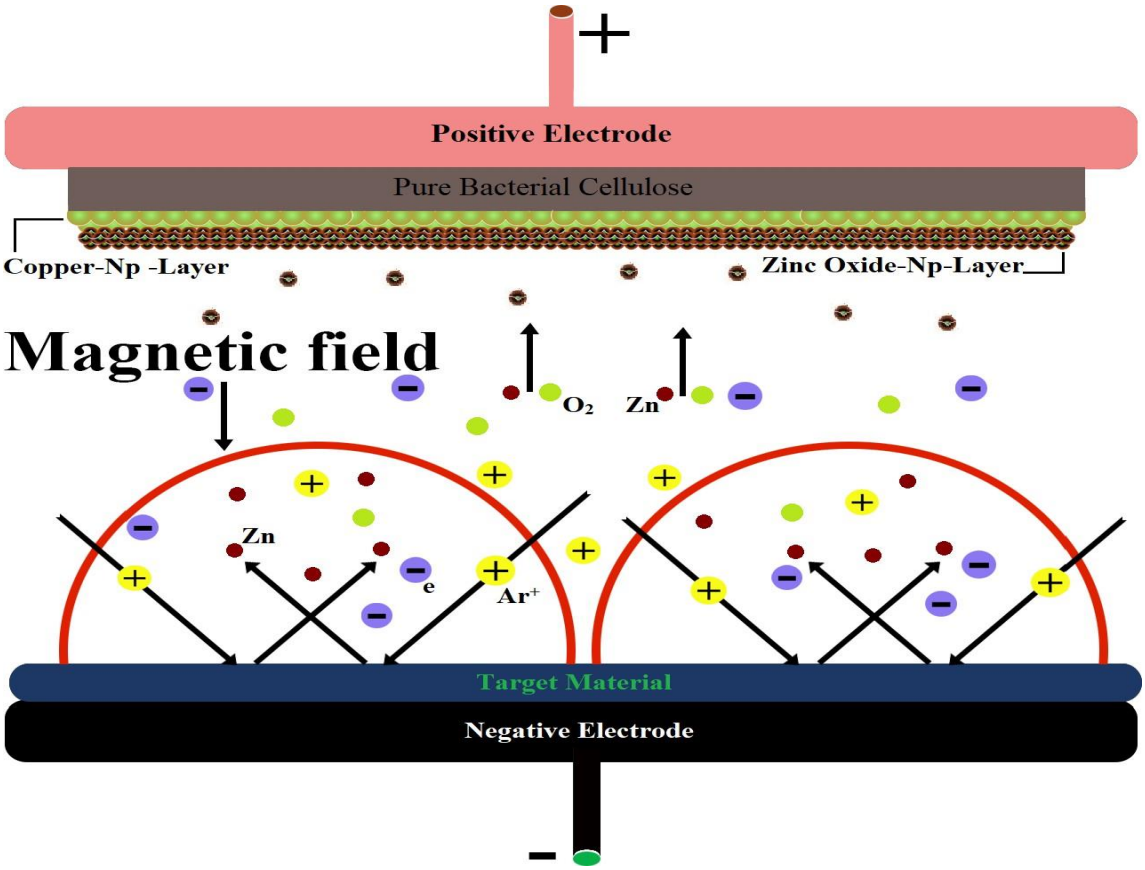

Figure 2. The process of the formation of copper and zinc oxide nanoparticles over the surface of pure bacterial cellulose by (DC and RF) magnetron sputter coating method.

2.4. Characterization

The morphological structure and chemical composition of layers of copper and zinc oxide nanoparticles deposited on bacterial cellulose were examined by X-ray photoelectron spectroscopy (XPS, Escalab 250Xi, Thermo Scientific Escalab, Waltham, MA, USA), energy-dispersive X-ray spectroscopic (EDS, version, S-4800, Hitachi, Tokyo, Japan) and X-ray diffraction (XRD, Bruker AXS D8, Berlin, Germany). The range of detection for XRD analysis was set to (1–90)/2θ. Similarly, ultraviolet resistance characteristics of the copper and zinc oxide nanoparticles on the bacterial cellulose were examined by an ultraviolet transmittance analyzer (UV-1000F, Lapsphere, NH, USA). In order to follow the standard method (GB/T18830-2009) of the UV-resistance test, all samples were stored for 24 h at 20 °C with 65% humidity rate, prior to measuring the UV-resistance test. The measuring indexes T (UVA), T(UVB) and ultraviolet protection factor (UPF) were taken into account to evaluate the values, and the test was performed in triplicate to get the aggregate values. Similarly, to find out the antistatic characteristics of coated (Cu/ZnO) bacterial cellulose, the static-honest meter (YG-B 342D; China) was employed. In order to follow the procedure, all samples were placed in a standard atmosphere with a temperature of 20 °C and 35% humidity rate for 24 h. The voltage was set 13 kV, and each sample was tested in triplicate to get aggregated values.

To find out the antibacterial effects of the bacterial cellulose/copper nanocomposite, bacterial cellulose/copper/zinc oxide nanocomposite was quantitively assessed in triplicate by standard Gram-positive bacteria (*S. aureus*) ATCC 6538 and Gram-negative bacteria (*E. coli*) ATCC 22125 [54]. First of all, to determine *E.coli* and *S. aureus* bacterial growth, 400 mL phosphate-buffered saline (PBS),

200 mL lysogeny broth (LB), 200 mL Lennox agar (LA), 200 mL tryptone soya agar (TSA) and 200 mL tryptone soya broth (TSB) solutions were made and autoclaved for 4 h at 70 °C. The 200 mL solution of TSA for *S. aureus* (and similarly, the 200 mL solution of LA for *E. coli*) was equally coated on 5 graded square plates and kept it at 25 °C for 12 h. After that, triplicate samples of BC/Cu and BC/Cu/ZnO (16 mm diameter) were placed separately into head-to-head wells of 24-well plates; for a control, another 24-well dish was prepared without samples. After that, each well was filled by a 100 µL aliquot of phosphate-buffered saline (PBS). This PBS solution was comprised of 1.3×10^8 colony forming units (CFU)/mL of bacteria which were extracted by the suspension of 3 mL tryptone soya broth (TSB) and lysogen broth (LB) bacteria respectively. Subsequently, both sample and control plates were filled with 0.91 mL of sterile phosphate-buffered saline. To confirm the proper resuspension of bacteria, all dishes were actively stirred for 10 s. Then, we did a 1:10 serial dilution (100 µL in 0.9 mL aliquots of phosphate-buffered saline) of each well 5 times, and 10 µL of the undiluted well was taken while each diluted well was individually coated on graded lines of tryptone soya agar (TSA) and Lennox agar (LA) square plates. Then these plates were kept for 18 h in an incubator at 37 °C. The growth rate was calculated by the ratio of CFU/mL of the sampled dish with the ratio of the resultant control. The minimum exposure limit was 100 CFU/well (established using the coated 10 µL aliquot from the 1 mL undiluted well), and the exposure limit range of *E.coli* microbial growth was 2.63% for BC/Cu and 1.55% for BC/Cu/ZnO. Similarly, the exposure limit range of *S. aureus* microbial growth was 3.15% for BC/Cu and 1.89 % for BC/Cu/ZnO. The inhibitions were the outcomes of antibacterial compounds regarding the samples of BC/Cu and BC/Cu/ZnO, and the concentration decrease from the diluted towards the original sample solution on graded TSA and LA square plates respectively. If the concentration of potential antibacterial compound reduced from a certain value, then the microorganism growth increased; with an increased concentration of antibacterial compound, minimal growth was observed. If specific antimicrobial characteristics of sub-categoric metallics of Zn and Cu are taken into consideration, the bactericidal properties of metallic films can be linked to their abilities to ionize in a given environment. The standard potentials of ionization are 0.76 V and 0.52 V for zinc and copper, regarding the development of monovalent ions; and for divalent ions: +0.34 V. Therefore, the composition of copper and zinc oxide nanoparticles on the surface of bacterial cellulose shows that BC/Cu/ZnO composite has a good antibacterial property and can be used as an antibacterial candidate.

3. Results and Discussion

3.1. XPS Analysis

XPS test was employed to find out the surface morphology and chemical composition of bacterial cellulose/copper/zinc oxide nanocomposite. It was also to confirm the oxidation of the copper nanoparticle film deposited in a highly pressurized oxygen environment over the surface of bacteria cellulose by magnetron sputter coating and the formation of protective zinc oxide nanoparticles layer over BC/Copper substrate [55].

Figure 3a illustrates the full spectrum of Cu2p peaks, the O1s peak and the C1s peak for the nanocomposite sample of bacterial cellulose/copper. C1s peak mainly represents the fibrous structure of the sample. In addition, the peak of C1s originally shows carbon from the bacterial cellulose, which confirms the oxidation of copper in spectra [56]. O1s represent that copper was oxidized from the ambient atmosphere, in which a possible reason may also be a residue of oxygen in Ar or O_2 valves in a sputter coating machine [57]. A combination of copper and oxygen may produce a different form of Cu_2O_3, Cu_2O, CuO and others. In Figure 3b,c the peaks corresponding to Cu+ (932.07 and 952.03 eV) and Cu2+ (934.08, 943.83, 954.08 and 962.23 eV) with O1s (531.13 eV) illustrate the exitance of copper with high oxidizing states and confirm the oxidation over the surface of sample [58].

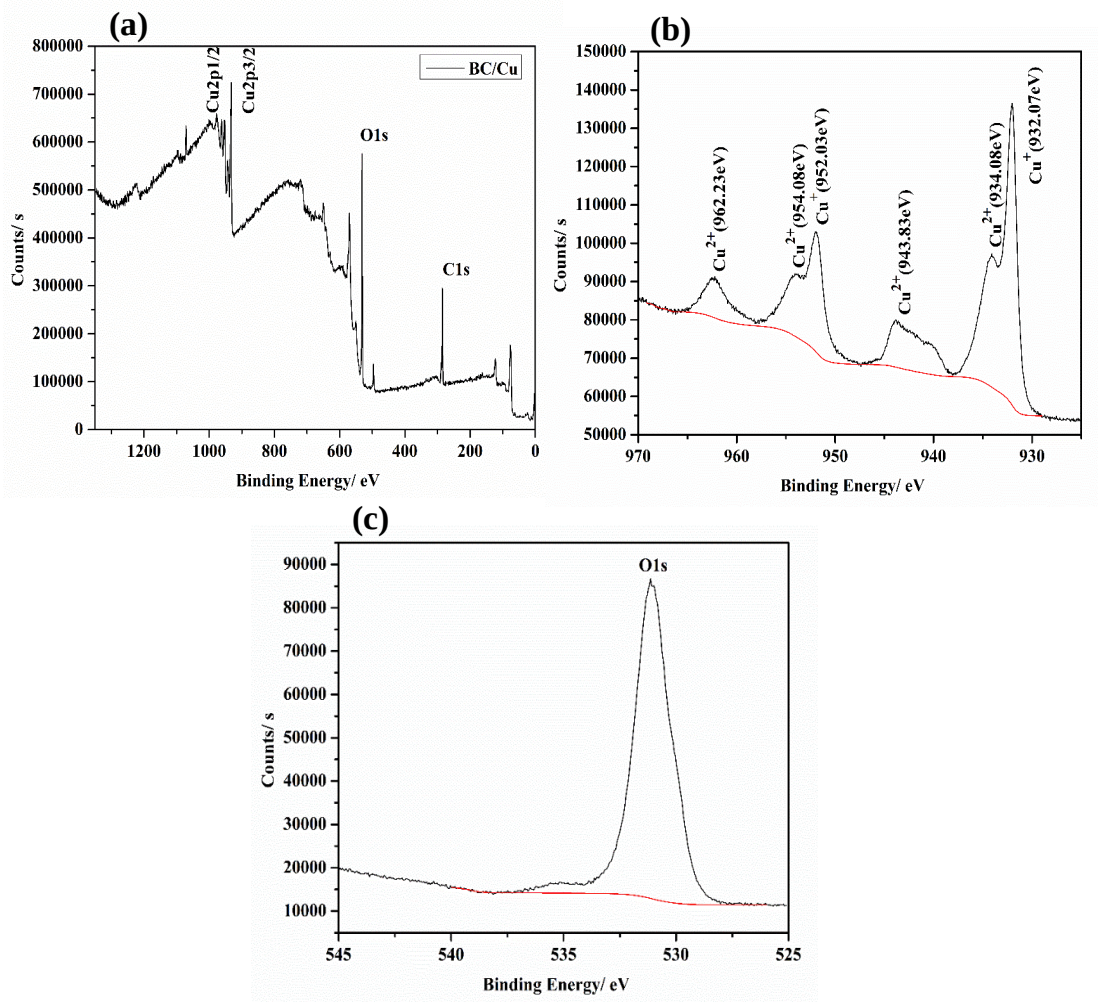

Figure 3. XPS peak representations of bacterial cellulose/copper nanocomposite: (**a**) XPS full spectrum; (**b**) copper peaks; (**c**) oxygen peak.

In high resolution XPS spectra according to Figure 4, the peaks attributed to Cu2p, O1s and Zn2p are illustrate the composition of the bacterial cellulose/copper/zinc oxide nanocomposite. All peaks in Figure 4a describe the elements zinc, copper, oxygen and carbon, and no obvious peak is found regarding other elements. In Figure 4c, the distinctive peaks of copper can be seen very clearly at 931.8 and 951.4 eV, which correspond to $Cu_{2p}3/2$ and $Cu_{2p}1/2$ of Cu+. That shows that copper is found in oxide form; that is perhaps due to the introduction of oxygen during the RF sputter coating method [59].

In Figure 4a, the peaks $Zn_{2p}1/2$, $Zn_{2p}3/2$, Zn3s, Zn3p, Zn3d and Zn(LLM) represent the presence of zinc elements, in which Zn2p peaks reveals the strongest characteristic peaks value. In addition, $Zn_{2p}1/2$ peaks, $Zn_{2p}3/2$ peaks and O1s peaks correspond to 1045.13, 1022.13 (Figure 4b) and 530.63 eV (Figure 4d) respectively, which proves that in the nanocomposite sample, zinc is found in the form of zinc oxide [60].

According to the comparison of Figures 3 and 4, it can be easily observed that spectral peak areas of bacterial cellulose/copper nanocomposite are higher than for the bacterial cellulose/copper/zinc oxide nanocomposite, which confirms that the copper layer is fully covered by the protective layer of zinc oxide.

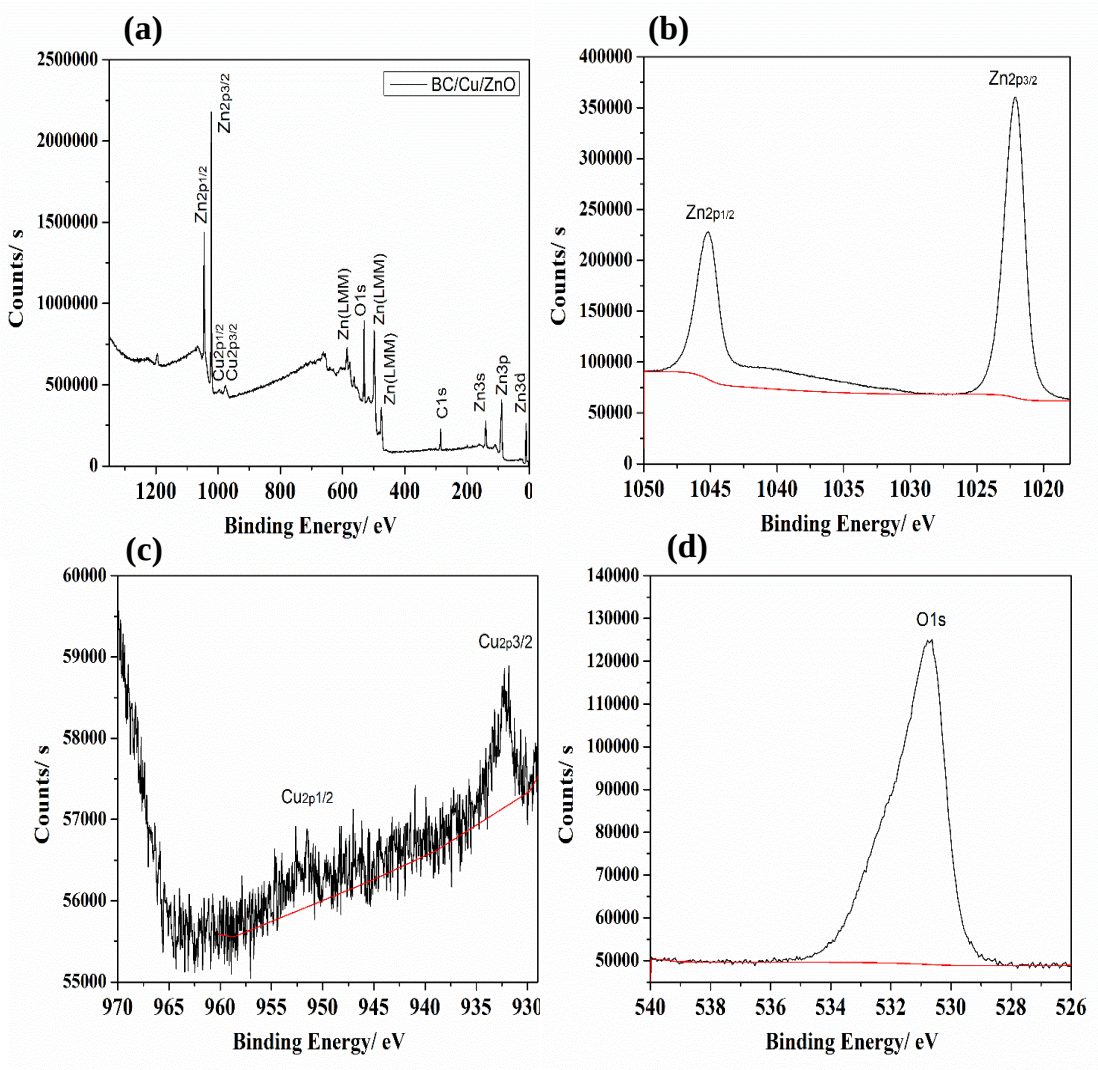

Figure 4. XPS peak representations of bacterial cellulose/copper/zinc oxide nanocomposite: (**a**) XPS full spectrum; (**b**) zinc peaks; (**c**) copper peaks; (**d**) oxygen peak.

3.2. EDS Analysis

Energy-dispersive X-ray spectroscopy (EDS) was employed to determine the elemental composition and mapping. The distribution of elements in bacterial cellulose/copper nanocomposite and bacterial cellulose/copper/zinc oxide nanocomposite were observed by FE-SEM (S-4800, Hitachi, Japan). From Figure 5a,b, it can be observed that the surface of bacterial cellulose is successively modified by copper nanoparticles with the help of DC magnetron sputter coating technique. The element mapping of copper, carbon and oxygen on the surface of bacterial cellulose can also be seen from Figure 5c–f, whereas Figure 5g describes the distinguished peaks of elements and shows the presence of elements in a uniform pattern [15].

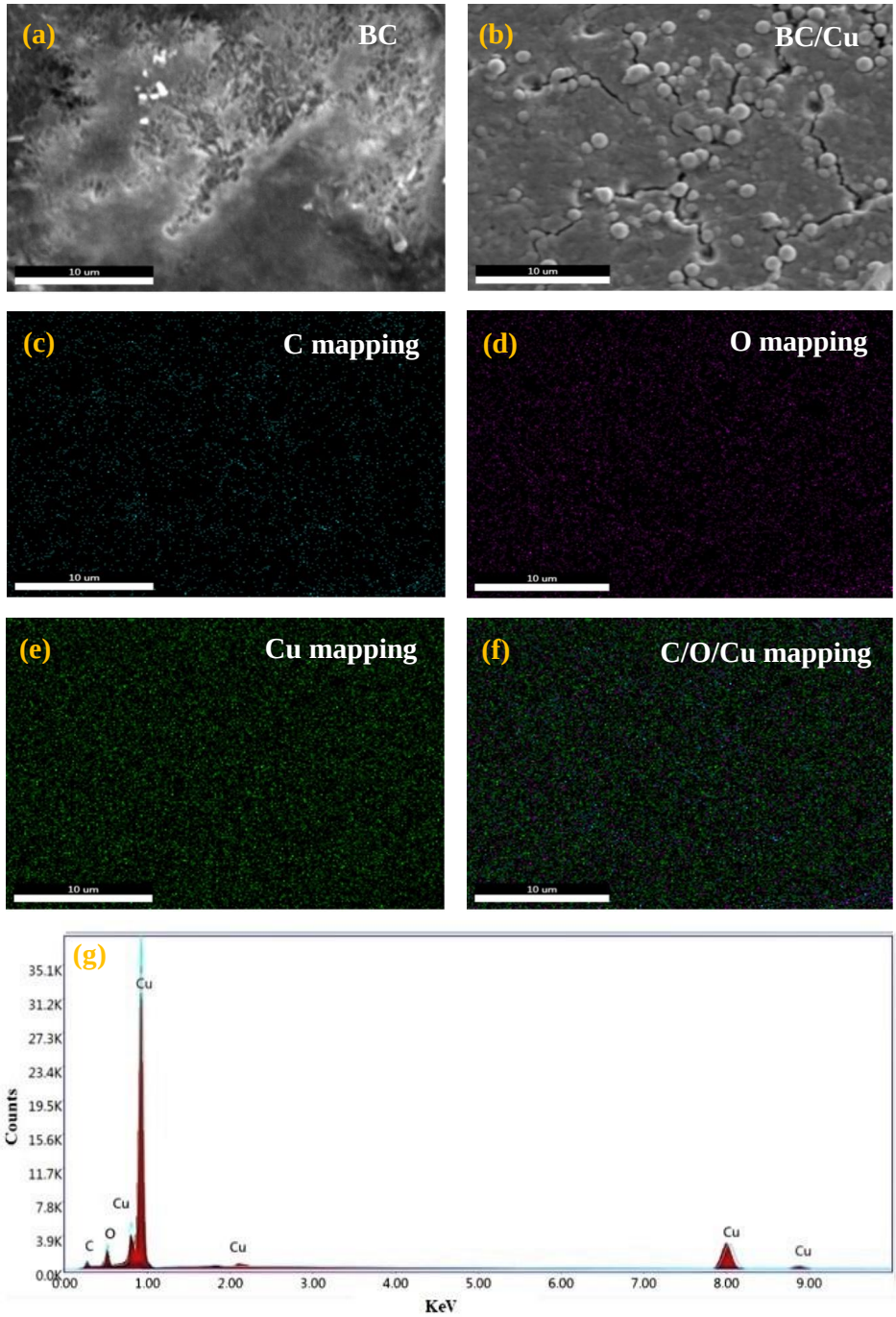

Figure 5. Elemental distribution in bacterial cellulose/copper nanocomposite; EDS-SEM (**a**–**f**) representation of element mapping; (**g**) distinguished peaks of elements.

Similarly, in Figure 6a it can be observed that bacterial cellulose is first modified by copper nanoparticles with the help of DC magnetron sputter coating and then zinc oxide nanoparticles using RF reactive sputter coating technique. Figure 6a–f describes the carbon, oxygen, copper and zinc element mapping over the surface of bacterial cellulose, while Figure 6g describes the peaks of elements and shows the presence of elements with a unique pattern [15,61]. The most important thing that is observed in both Figures 5g and 6g is a peak of oxygen in the EDS spectra, which confirms that copper and zinc are found in their oxidized forms in both nanocomposites.

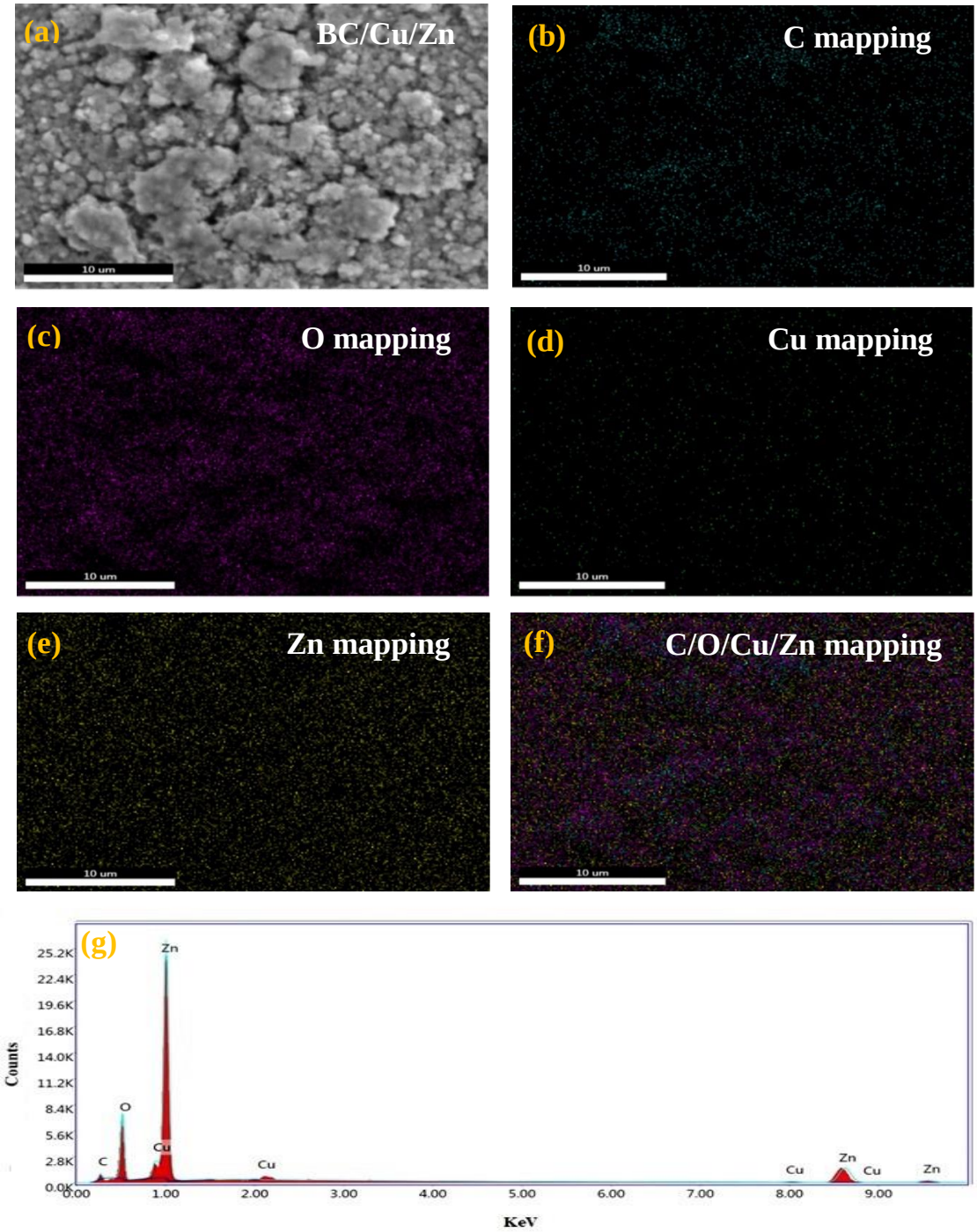

Figure 6. Element distributions in bacterial cellulose/copper/zinc oxide nanocomposite; EDS-SEM (**a**–**f**) representation of element mapping; (**g**) distinguished peaks of elements.

In addition, in the sample of bacterial cellulose/copper the mapping of carbon illustrates that the carbon peak comes from the source of pure bacterial cellulose, which confirms the oxidation of copper [56]. In contrast, in the sample of bacterial cellulose/copper/zinc oxide, the peak of carbon represents that carbon is overlapped with oxygen, copper and zinc, demonstrating the uniform distribution of zinc, oxygen and copper elements in the carbon matrix [62,63].

Table 1 reveals the atomic percentages of elements within the two different nanocomposites. The atomic contents in bacterial cellulose/copper nanocomposite are: carbon (17.64%), oxygen (14.08%) and copper (68.28%). In addition, the atomic contents in bacterial cellulose/copper/zinc oxide

nanocomposite are: carbon (16.44%), oxygen (38.87%), copper (1.22%) and zinc (43.47%). It can be clearly observed that carbon content originally came from the bacterial cellulose did not change significantly. However, the atomic content ratio of oxygen and zinc in bacterial cellulose/copper/zinc oxide nanocomposite is 2:3, while the copper content value is only 1.22%, which demonstrates that the copper surface is successively protected by a zinc oxide layer in this nanocomposite.

Table 1. Atomic content percentages of different elements in nanocomposites.

Samples	Atomic Content % of Elements			
	Carbon	Oxygen	Copper	Zinc
Bacterial Cellulose/Copper	17.64	14.08	68.28	
Bacterial Cellulose/Copper/Zinc Oxide	16.44	38.87	1.22	43.47

3.3. XRD Analysis

Figure 7 illustrates the XRD patterns of pure bacterial cellulose, bacterial cellulose/copper nanocomposite and bacterial cellulose/copper/zinc oxide nanocomposite. Figure 7a illustrates the sample of pure bacterial cellulose with distinguished peaks at 14.6°, 16.9° and 22.8°, which correspond to crystallographic plane values (100), (010) and (110) respectively [64,65]. Similarly, in Figure 7b, it can be seen that the peak at 36.90° and 43.7° correspond to (002) and (220) plane reflection values of copper oxide and copper respectively in the sample of bacterial cellulose/copper nanocomposite [66].

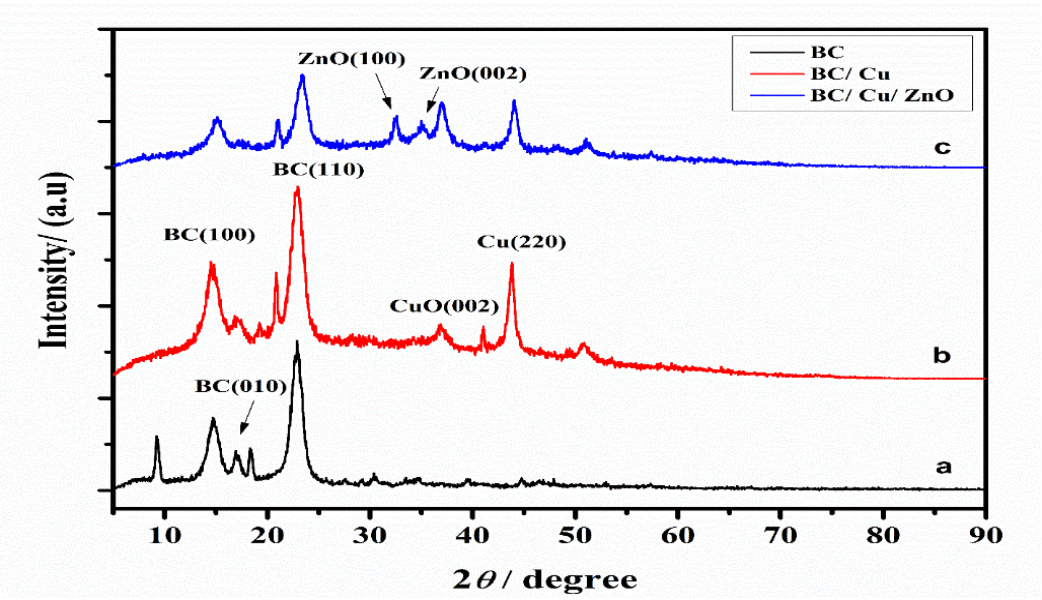

Figure 7. The X-ray diffraction (XRD) representations of three samples: (**a**) bacterial cellulose; (**b**) bacterial cellulose/copper nanocomposite; (**c**) bacterial cellulose/copper/zinc oxide nanocomposite.

Further, it can also be observed that the peak of copper in bacterial cellulose/copper nanocomposite sample is narrow and pointed, which shows that it has a high degree of crystallinity, while other peaks are similar to those of pure bacterial cellulose. Moreover, Figure 7c is describing the distinguished peaks of bacterial cellulose coated with copper and zinc oxide nanoparticles. The diffraction peaks at 32.6° and 35° correspond to (100) and (002) planes values of bacterial cellulose/copper/zinc oxide nanocomposite, while the other peaks are similar to Figure 7a,b the bacterial cellulose/copper sample [67].

It can also be seen from Figure 7b,c that bacterial cellulose with the copper nanoparticle sputter coating shows the higher intensity of crystallinity. In contrast, bacterial cellulose with zinc oxide nanoparticle sputter coating shows very low peak values of crystallinity because of the RF sputter

coating of zinc oxide on the copper layer. Thus, it clearly shows that the copper layer is completely covered by zinc oxide nanoparticles, which provide protection to the copper layer from further oxidation.

3.4. Antistatic Analysis

The antistatic properties of bacterial cellulose/copper and bacterial cellulose/copper/zinc oxide nanocomposites were determined by the static honest meter (YG-B 342D; Shanghai, China), and values in Table 2 illustrate their antistatic characteristics. If the static half period values increase, it means the material has higher antistatic properties, while instantaneous electrostatic voltage works oppositely in terms of values. According Table 2, the comparison between bacterial cellulose/copper nanocomposite and bacterial cellulose/copper/zinc oxide nanocomposite shows that BC/Copper has sufficient antistatic properties, but BC/Copper/Zinc oxide has excellent antistatic properties in terms of average values of static half period and instantaneous electrostatic voltage. In addition, the results from our previous work are also presented in Table 2 to give a comparison between these materials, which shows that bacterial cellulose/copper and bacterial cellulose/copper/zinc oxide nanocomposites could also be good candidates for antistatic materials.

Table 2. Comparison of different nanocomposite materials in terms of antistatic characteristics.

Nanocomposite Materials	Static Half Period/s	Instantaneous Electrostatic Voltage/V	Reference
Polyester fabric/Ag	0.51 ± 0.23	188 ± 9.83	[56]
Polyester fabric/Ag_2O	4.658 ± 0.39	380 ± 8.94	
Polyester fabric/Ag/ZnO	70.34 ± 10.42	565 ± 5.48	
Polyester fabric/Ag2O/ZnO	25.83 ± 3.58	315 ± 5.48	
Bacterial Cellulose/Copper	3.386 ± 0.56	259.66 ± 5.50	This work
Bacterial Cellulose/Copper/Zinc Oxide	51.50 ± 4.10	349.3 ± 6.02	

3.5. Ultraviolet Resistance Analysis

The ultraviolet resistance properties of bacterial cellulose/copper and bacterial-cellulose/copper/zinc oxide nanocomposites were determined by the ultraviolet transmittance analyzer (UV-1000F, Lapsphere, NH, USA). The results in Table 3 are describing the UV-resistance characteristics of different nanocomposites. Ultraviolet resistance characteristics depend on the percentage values of T (UVA) and T (UVB) and the UPF value. If material indicates the lower percentage value of T (UVA) and T (UVB), it means that the material has good ultraviolet resistance properties, while the higher identical value of ultraviolet protection factor (UPF) represents the material has enhanced toward excellent ultraviolet resistance characteristics. In Table 3, the comparison values of our targets, bacterial cellulose/copper and bacterial cellulose/copper/zinc oxide nanocomposites clearly show that the addition of zinc oxide nanoparticles on bacterial cellulose/copper surface enhances its ultraviolet resistance property. This may occur because of the addition of the zinc oxide layer, that not only increases the thickness of material but also protects further from oxidation and ultraviolet radiation according to results given in Table 3.

Table 3. Comparison of different nanocomposite materials in terms of ultraviolet resistance characteristics.

Nanocomposite Materials	T(UVA)/%	T(UVB)/%	UPF	Reference
Polyester fabric/Ag	3.52 ± 0.02	2.69 ± 0.05	35.26 ± 0.61	[56]
Polyester fabric/Ag_2O	4.36 ± 0.43	3.67 ± 0.18	26.70 ± 1.64	
Polyester fabric/Ag/ZnO	3.94 ± 0.07	3.55 ± 0.14	27.68 ± 1.21	
Polyester fabric/Ag2O/ZnO	3.86 ± 0.24	3.21 ± 0.01	30.37 ± 0.20	
Bacterial Cellulose/Copper	0.22 ± 0.01	0.12 ± 0.02	918.27 ± 1.90	This work
Bacterial Cellulose/Copper/Zinc Oxide	0.16 ± 0.02	0.07 ± 0.01	1850.33 ± 2.12	

In summary, literature values of our previous work are also reported here to present a comparison between these materials, which shows that bacterial cellulose/copper and bacterial cellulose/copper/zinc oxide nanocomposites possess good ultraviolet resistance characteristics, and can be used in the application of ultraviolet-resistive materials.

3.6. Antibacterial Analysis

The antibacterial properties of bacterial cellulose/copper and bacterial cellulose/copper/zinc oxide nanocomposites and pure bacterial cellulose were examined by the culture count method of *E. coli* and *S. aureus* bacterial growth. The antibacterial characteristics of a material depend upon the ascending and descending growth rate of microbial activity; i.e., if the growth rate is low, the material has an excellent antibacterial property, and vice versa. In addition, this growth rate is calculated by the following equation.

$$G.R\ \% = \left[\frac{A - B}{A}\right] \times 100 \quad (1)$$

where G.R = growth rate, A = number of bacterial colonies from a controlled sample and B = number of bacterial colonies from prepared nanocomposite material.

The Table 4 clearly illustrates that the addition of copper and zinc oxide on bacterial cellulose enhances its antibacterial characteristics; moreover, with the comparison of different samples from previous literature, it also shows that these new nanocomposites have significant values of antibacterial activity. In addition, it was observed that the growth rate of *E. coli* bacteria was very low compared to *S. aureus* in terms of both bacterial cellulose/copper and bacterial cellulose/copper/zinc oxide nanocomposites. However, pure bacterial cellulose shows no special antibacterial characteristics. The values of the *E. coli* bacterial growth rate for bacterial cellulose/copper and bacterial cellulose/copper/zinc oxide nanocomposite demonstrate 97.37% and 98.45% antibacterial activity, respectively. Similarly, the values against *S. aureus* bacterial growth represent that bacterial cellulose/copper and bacterial cellulose/copper/zinc oxide nanocomposites show 96.85% and 98.11% antibacterial activity, respectively. The difference between *E. coli* and *S. aureus* bacterial growth rates for high and low antibacterial characteristics could be due to the morphological structure of the bacterial cell wall. In addition, the difference represents the fact that *S. aureus* has a thick peptidoglycan layer in the outer membrane compared to *E. coli*, which may cause a reduction in the mass diffusion of nanoparticles into *S. aureus* bacteria; that could be a possible reflection of low antibacterial characteristics of the nanocomposite against *S. aureus*. Conclusively, both bacterial cellulose/copper and bacterial cellulose/copper/zinc oxide nanocomposites have good antibacterial properties and should be antibacterial candidates for many applications in daily life.

Table 4. Different nanocomposite materials' antibacterial characteristics in terms of *Escherichia coli* and *Staphylococcus aureus* bacterial growth.

Samples	Bacterial Growth (%)		
	***E. Coli* (ATCC 22125)**	***S. aureus* (ATCC 6538)**	**Reference**
FPEI-A	5.99	7.89	[61]
FPEI-AZ	5.45	6.86	
FPEI-AZC	4.9	5.83	
PMC-A	2.49	1.85	
PMC-AZ	2.22	1.84	
PMC-AZC	1.95	1.83	
Pure Bacterial Cellulose	100	100	This work
Bacterial Cellulose/Copper	2.63	3.15	
Bacterial Cellulose/Copper/Zinc Oxide	1.55	1.89	

4. Conclusions

In conclusion, we successively fabricated copper and zinc oxide nanoparticles on bacterial cellulose using direct current (DC) magnetron and radio frequency (RF) reactive sputter coating methods to make a bacterial cellulose/copper/zinc oxide nanocomposite. The target copper and zinc were 99.99% pure during the sputter coating; copper nanoparticles were sputtered for 60 min and zinc nanoparticles were sputtered for 30 min in the presence of argon gas. In the case of zinc nanoparticle sputter coating, oxygen was pumped to make the layer of zinc oxide nanoparticles. Conclusively, our study by XPS, XRD and EDS reveals that the outer layer of zinc oxide on copper with bacterial cellulose not only provides protection from oxidation for copper but also enhances the ultraviolet resistance, and antistatic and antibacterial properties of this nanocomposite. Meanwhile, this novel bacterial cellulose/copper/zinc oxide nanocomposite shows the best values of UV-resistance (T.VUA%; 0.16 ± 0.02, T.VUB%; 0.07 ± 0.01, UPF; 1850.33 ± 2.12), antistatic activity (S.H. P; 51.50 ± 4.10, I.E. V; 349.33 ± 6.02) and antibacterial activity (*E. coli*; 98.45% and *S. aureus*; 98.11%), which show that this green nanocomposite material can be effectively used functionally, technically, medically and in many daily life applications.

Author Contributions: Conceptualization, M.W. and Q.W.; methodology, M.W.; software, M.W. and M.H.; validation, M.W.; Q.W.; and A.N.; formal analysis, M.W.; M.M.; investigation, Q.W.; resources, M.W.; data curation, M.R.K.; writing—original draft preparation, M.W.; writing—review and editing, Q.W. and A.N.; visualization, M.W.; supervision, Q.W.; project administration, M.W.; funding acquisition, Q.W. All authors have read and agreed to the published version of the manuscript.

Funding: This research was funded by National first-class discipline program of Light Industry Technology and Engineering: LITE2018-21

Acknowledgments: This research is grateful to the nanocomposite materials with training of young academic scholars, whereas instruments support of Key Laboratory of Eco Textiles, Jiangnan University, Wuxi, Jiangsu, China.

Conflicts of Interest: The authors declare no conflict of interest.

References

1. Chen, D.; Chen, Q.; Ge, L.; Yin, L.; Fan, B.; Wang, H.; Lu, H.; Xu, H.; Zhang, R.; Shao, G. Synthesis and Ag-loading-density-dependent photocatalytic activity of Ag@TiO2 hybrid nanocrystals. *Appl. Surf. Sci.* **2013**, *284*, 921–929. [CrossRef]
2. Mishra, Y.K.; Mohapatra, S.; Singhal, R.; Avasthi, D.; Agarwal, D.C.; Ogale, S. Au–ZnO: A tunable localized surface plasmonic nanocomposite. *Appl. Phys. Lett.* **2008**, *92*, 043107. [CrossRef]
3. Barakat, A.N.; Al-Deyab, S.; Kim, H.Y. Synthesis and study of the photoluminescence and optical characteristics of Cd/CdO nanorods prepared by the electrospinning process. *Mater. Lett.* **2012**, *66*, 225–228. [CrossRef]
4. Geetha, D.; Kavitha, S.; Ramesh, P. A novel bio-degradable polymer stabilized Ag/TiO2 nanocomposites and their catalytic activity on reduction of methylene blue under natural sun light. *Ecotoxicol. Environ. Saf.* **2015**, *121*, 126–134. [CrossRef]
5. Lee, D.-S.; Chen, Y.-W. Nano Ag/TiO2 catalyst prepared by chemical deposition and its photocatalytic activity. *J. Taiwan Inst. Chem. Eng.* **2014**, *45*, 705–712. [CrossRef]
6. Bazant, P.; Kuritka, I.; Munster, L.; Kalina, L. Microwave solvothermal decoration of the cellulose surface by nanostructured hybrid Ag/ZnO particles: A joint XPS, XRD and SEM study. *Cellulose* **2015**, *22*, 1275–1293. [CrossRef]
7. Sun, F.; Qiao, X.; Tan, F.; Wang, W.; Qiu, X. One-step microwave synthesis of Ag/ZnO nanocomposites with enhanced photocatalytic performance. *J. Mater. Sci.* **2012**, *47*, 7262–7268. [CrossRef]
8. Chen, Y.-C.; Cheng, J.; Cheng, J.; Cheng, S. l-Arginine assisted preparation of Ag/ZnO nanocomposites with enhanced photocatalytic performance. *J. Mater. Sci. Mater. Electron.* **2015**, *26*, 2775–2781. [CrossRef]
9. Gunasekar, V.; Ponnusami, V. Plasmonic photocatalysis and kinetics of reactive dye degradation in aqueous solution using enzymatically synthesized Ag/ZnO. *J. Sol-Gel Sci. Technol.* **2015**, *74*, 84–93. [CrossRef]
10. Tamayo, L.; Azócar, M.; Kogan, M.; Riveros, A.; Páez, M. Copper-polymer nanocomposites: An excellent and cost-effective biocide for use on antibacterial surfaces. *Mater. Sci. Eng. C* **2016**, *69*, 1391–1409. [CrossRef]
11. Cady, C.N.; Behnke, J.L.; Strickland, A.D. Copper-Based Nanostructured Coatings on Natural Cellulose: Nanocomposites Exhibiting Rapid and Efficient Inhibition of a Multi-Drug Resistant Wound Pathogen,

A. baumannii, and Mammalian Cell Biocompatibility In Vitro. *Adv. Funct. Mater.* **2011**, *21*, 2506–2514. [CrossRef]
12. Yang, Y.; Huang, Q.; Payne, G.F.; Sun, S.; Wang, X. A highly conductive, pliable and foldable Cu/cellulose paper electrode enabled by controlled deposition of copper nanoparticles. *Nanoscale* **2019**, *11*, 725–732. [CrossRef] [PubMed]
13. Kishanji, M.; Mamatha, G.; Reddy, K.O.; Rajulu, A.V.; Madhukar, K. In situ generation of silver nanoparticles in cellulose matrix using Azadirachta indica leaf extract as a reducing agent. *Int. J. Polym. Anal. Charact.* **2017**, *22*, 734–740. [CrossRef]
14. Hannon, J.C.; Kerry, J.P.; Cruz-Romero, M.; Azlin-Hasim, S.; Morris, M.A.; Cummins, E. Assessment of the migration potential of nanosilver from nanoparticle-coated low-density polyethylene food packaging into food simulants. *Food Addit. Contam. Part A* **2016**, *33*, 167–178. [CrossRef]
15. Muthulakshmi, L.; Rajalu, A.V.; Kaliaraj, G.S.; Siengchin, S.; Parameswaranpillai, J.; Saraswathi, R. Preparation of cellulose/copper nanoparticles bionanocomposite films using a bioflocculant polymer as reducing agent for antibacterial and anticorrosion applications. *Compos. Part B Eng.* **2019**, *175*, 107177. [CrossRef]
16. Ullah, H.; Wahid, F.; Santos, H.A.; Khan, T. Advances in biomedical and pharmaceutical applications of functional bacterial cellulose-based nanocomposites. *Carbohydr. Polym.* **2016**, *150*, 330–352. [CrossRef]
17. Foresti, L.M.; Vázquez, A.; Boury, B. Applications of bacterial cellulose as precursor of carbon and composites with metal oxide, metal sulfide and metal nanoparticles: A review of recent advances. *Carbohydr. Polym.* **2017**, *157*, 447–467. [CrossRef]
18. Booshehri, A.Y.; Wang, R.; Xu, R. Simple method of deposition of CuO nanoparticles on a cellulose paper and its antibacterial activity. *Chem. Eng. J.* **2015**, *262*, 999–1008. [CrossRef]
19. Mu, J.; Shao, C.; Guo, Z.; Zhang, Z.; Zhang, M.; Zhang, P.; Chen, B.; Liu, Y. High Photocatalytic Activity of ZnO−Carbon Nanofiber Heteroarchitectures. *ACS Appl. Mater. Interfaces* **2011**, *3*, 590–596. [CrossRef]
20. Wu, J.; Xue, D. Progress of science and technology of ZnO as advanced material. *Sci. Adv. Mater.* **2011**, *3*, 127–149. [CrossRef]
21. Xu, S.; Wang, Z.L. One-dimensional ZnO nanostructures: Solution growth and functional properties. *Nano Res.* **2011**, *4*, 1013–1098. [CrossRef]
22. Pandimurugan, R.; Thambidurai, S. UV protection and antibacterial properties of seaweed capped ZnO nanoparticles coated cotton fabrics. *Int. J. Biol. Macromol.* **2017**, *105*, 788–795. [CrossRef] [PubMed]
23. Saravanan, D. UV protection textile materials. *AUTEX Res. J.* **2007**, *7*, 53–62.
24. Ranjan Das, B. UV radiation protective clothing. *Open Text. J.* **2010**, *3*, 14–21.
25. Parejo, P.G.; Zayat, M.; Levy, D. Highly efficient UV-absorbing thin-film coatings for protection of organic materials against photodegradation. *J. Mater. Chem.* **2006**, *16*, 2165–2169. [CrossRef]
26. Ghamsari, M.S.; Alamdari, S.; Han, W.; Park, H.-H. Impact of nanostructured thin ZnO film in ultraviolet protection. *Int. J. Nanomed.* **2017**, *12*, 207. [CrossRef]
27. Calvo, M.E.; Smirnov, J.R.C.; Míguez, H. Novel approaches to flexible visible transparent hybrid films for ultraviolet protection. *J. Polym. Sci. Part B Polym. Phys.* **2012**, *50*, 945–956. [CrossRef]
28. Rusdi, R.; Rahman, A.A.; Mohamed, N.S.; Kamarudin, N.; Kamarulzaman, N. Preparation and band gap energies of ZnO nanotubes, nanorods and spherical nanostructures. *Powder Technol.* **2011**, *210*, 18–22. [CrossRef]
29. Lee, Y.-J.; Ruby, D.S.; Peters, D.W.; McKenzie, B.B.; Hsu, J.W.P. ZnO Nanostructures as Efficient Antireflection Layers in Solar Cells. *Nano Lett.* **2008**, *8*, 1501–1505. [CrossRef]
30. Tsuzuki, T.; Wang, X.; Ali, N.; El-Mohamedy, R. Nanoparticle Coatings for UV Protective Textiles. *Res. J. Text. Appar.* **2010**, *14*, 9–20. [CrossRef]
31. Pospíšil, J.; Nešpůrek, S. Photostabilization of coatings. Mechanisms and performance. *Prog. Polym. Sci.* **2000**, *25*, 1261–1335. [CrossRef]
32. Çakır, B.A.; Budama, L.; Topel, Ö.; Hoda, N. Synthesis of ZnO nanoparticles using PS-b-PAA reverse micelle cores for UV protective, self-cleaning and antibacterial textile applications. *Colloids Surf. A Physicochem. Eng. Asp.* **2012**, *414*, 132–139. [CrossRef]
33. Han, Y.B.; Han, J.B.; Ding, S.; Chen, D.J.; Wang, Q.Q. Optical nonlinearity of ZnO microcrystallite enhanced by interfacial state. *Opt. Express* **2005**, *13*, 9211–9216. [CrossRef]
34. Niu, Q.-X.; Liu, Y.-J.; Song, D.-J.; Gao, Y.-J.; Dai, C.-L.; Yang, H.-W. Research of anti-ultraviolet nano-film structure based on the FDTD method. *Optik* **2016**, *127*, 539–543. [CrossRef]

35. Wang, Y.; Yao, J.; Jia, G.; Lei, H. Optical Prosperities of Ag-ZnO Composition Nanofilm Synthesized by Chemical Bath Deposition. *Acta Phys. Pol. A* **2011**, *119*, 451–454. [CrossRef]
36. Iervolino, G.; Zammit, I.; Vaiano, V.; Rizzo, L. Limitations and Prospects for Wastewater Treatment by UV and Visible-Light-Active Heterogeneous Photocatalysis: A Critical Review. *Top. Curr. Chem.* **2020**, *378*, 7. [CrossRef]
37. Wang, J.; Fan, X.; Zhou, Z.; Tian, K. Preparation of Ag nanoparticles coated tetrapod-like ZnO whisker photocatalysts using photoreduction. *Mater. Sci. Eng. B* **2011**, *176*, 978–983. [CrossRef]
38. Lu, W.; Gao, S.; Wang, J. One-Pot Synthesis of Ag/ZnO Self-Assembled 3D Hollow Microspheres with Enhanced Photocatalytic Performance. *J. Phys. Chem. C* **2008**, *112*, 16792–16800. [CrossRef]
39. Kim, K.; Lee, D.-H.; Lee, S.Y.; Jang, G.-E.; Kim, J.-S. Effect of Ag/Al co-doping method on optically p-type ZnO nanowires synthesized by hot-walled pulsed laser deposition. *Nanoscale Res. Lett.* **2012**, *7*, 273. [CrossRef] [PubMed]
40. Wei, Q.; Xu, Q.; Cai, Y.; Gao, W.; Bo, C. Characterization of polymer nanofibers coated by reactive sputtering of zinc. *J. Mater. Process. Technol.* **2009**, *209*, 2028–2032. [CrossRef]
41. Waykar, R.G.; Pawbake, A.; Kulkarni, R.R.; Jadhavar, A.A.; Funde, A.; Waman, V.S.; Pathan, H.M.; Jadkar, S. Influence of RF power on structural, morphology, electrical, composition and optical properties of Al-doped ZnO films deposited by RF magnetron sputtering. *J. Mater. Sci. Mater. Electron.* **2015**, *27*, 1134–1143. [CrossRef]
42. Ramazanov, S.M.; Kurbanov, M.K.; Safaraliev, G.K.; Bilalov, B.A.; Kargin, N.I.; Gusev, A.S. Structural properties of the epitaxial (SiC) 1− x (AlN) x solid solution films fabricated by magnetron sputtering of SiC-Al composite targets. *Tech. Phys. Lett.* **2014**, *40*, 300–302. [CrossRef]
43. Li, H.T.; Wang, T.; Wang, Q. Composition and residual stress analysis of Ti-Si/(Ti-Si)xN film on Mg–Al alloy substrate prepared by magnetron sputtering. *Mater. Res. Innov.* **2015**, *19*, 1268–1271. [CrossRef]
44. Chen, S.; Zhou, B.; Hu, W.; Zhang, W.; Yin, N.; Wang, H. Polyol mediated synthesis of ZnO nanoparticles templated by bacterial cellulose. *Carbohydr. Polym.* **2013**, *92*, 1953–1959. [CrossRef]
45. Klemm, D.; Schumann, D.; Udhardt, U.; Marsch, S. Bacterial synthesized cellulose—Artificial blood vessels for microsurgery. *Prog. Polym. Sci.* **2001**, *26*, 1561–1603. [CrossRef]
46. Yan, Z.; Chen, S.; Wang, H.; Wang, B.; Jiang, J. Biosynthesis of bacterial cellulose/multi-walled carbon nanotubes in agitated culture. *Carbohydr. Polym.* **2008**, *74*, 659–665. [CrossRef]
47. Wen, L.; Ma, Y.; Dai, B.; Zhou, Y.; Liu, J.; Pei, C. Preparation and dielectric properties of SiC nanowires self-sacrificially templated by carbonated bacterial cellulose. *Mater. Res. Bull.* **2013**, *48*, 687–690. [CrossRef]
48. Yu, H.-Y.; Chen, G.-Y.; Wang, Y.-B.; Yao, J. A facile one-pot route for preparing cellulose nanocrystal/zinc oxide nanohybrids with high antibacterial and photocatalytic activity. *Cellulose* **2014**, *22*, 261–273. [CrossRef]
49. Wu, J.; Zheng, Y.; Song, W.; Luan, J.; Wen, X.; Wu, Z.; Chen, X.; Wang, Q.; Guo, S. In situ synthesis of silver-nanoparticles/bacterial cellulose composites for slow-released antimicrobial wound dressing. *Carbohydr. Polym.* **2014**, *102*, 762–771. [CrossRef]
50. Lv, P.; Wei, A.; Li, D.; Lucia, L.; Wei, Q.; Wang, Y.; Zhang, J. Copper nanoparticles-sputtered bacterial cellulose nanocomposites displaying enhanced electromagnetic shielding, thermal, conduction, and mechanical properties. *Cellulose* **2016**, *23*, 3117–3127. [CrossRef]
51. Long, C.; Qi, D.; Wei, T.; Yan, J.; Jiang, L.; Fan, Z. Nitrogen-Doped Carbon Networks for High Energy Density Supercapacitors Derived from Polyaniline Coated Bacterial Cellulose. *Adv. Funct. Mater.* **2014**, *24*, 3953–3961. [CrossRef]
52. Zhou, T. Electrically conductive bacterial cellulose composite membranes produced by the incorporation of graphite nanoplatelets in pristine bacterial cellulose membranes. *Express Polym. Lett.* **2013**, *7*, 756–766. [CrossRef]
53. Czaja, W.; Romanovicz, D.; Brown, R.M. Structural investigations of microbial cellulose produced in stationary and agitated culture. *Cellulose* **2004**, *11*, 403–411. [CrossRef]
54. Mohamed, A.; El-Naggar, M.E.; Shaheen, T.I.; Hassabo, A. Laminating of chemically modified silan based nanosols for advanced functionalization of cotton textiles. *Int. J. Boil. Macromol.* **2017**, *95*, 429–437. [CrossRef]
55. Hou, H.; Jing, M.; Yang, Y.; Zhang, Y.; Song, W.; Yang, X.; Chen, J.; Chen, Q.; Ji, X. Antimony nanoparticles anchored on interconnected carbon nanofibers networks as advanced anode material for sodium-ion batteries. *J. Power Sour.* **2015**, *284*, 227–235. [CrossRef]

56. Yuan, X.; Xu, W.; Huang, F.; Chen, N.; Wei, Q. Polyester fabric coated with Ag/ZnO composite film by magnetron sputtering. *Appl. Surf. Sci.* **2016**, *390*, 863–869. [CrossRef]
57. Su, J.; Liu, Y.; Jiang, M.; Zhu, X. Oxidation of copper during physical sputtering deposition: Mechanism, avoidance and utilization. *arXiv* **2014**, arXiv:1412.2031.
58. Kim, D.-W.; Rhee, K.-Y.; Park, S.-J. Synthesis of activated carbon nanotube/copper oxide composites and their electrochemical performance. *J. Alloys Compd.* **2012**, *530*, 6–10. [CrossRef]
59. Sun, S.; Zhang, X.; Song, X.-P.; Liang, S.; Wang, L.; Yang, Z. Bottom-up assembly of hierarchical Cu2O nanospheres: Controllable synthesis, formation mechanism and enhanced photochemical activities. *CrystEngComm* **2012**, *14*, 3545. [CrossRef]
60. Moulder, J.F.; Stickle, W.S.; Sobol, P.E.; Bomben, K.D. *Handbook of X-Ray Photoelectron Spectroscopy*; Perkin-Elmer Corporation: Eden Prairie, MN, USA, 1992.
61. Hassabo, A.; El-Naggar, M.E.; Mohamed, A.L.; Hebeish, A. Development of multifunctional modified cotton fabric with tri-component nanoparticles of silver, copper and zinc oxide. *Carbohydr. Polym.* **2019**, *210*, 144–156. [CrossRef]
62. Guo, S.-P.; Li, C.-X.; Chi, Y.; Ma, Z.; Xue, H.-G. Novel 3-D network SeS/NCPAN composites prepared by one-pot in-situ solid-state method and its electrochemical performance as cathode material for lithium-ion battery. *J. Alloys Compd.* **2016**, *664*, 92–98. [CrossRef]
63. Chow, L.; Lupan, O.; Chai, G.; Khallaf, H.; Ono, L.; Cuenya, B.R.; Tiginyanu, I.; Ursaki, V.; Sontea, V.; Schulte, A. Synthesis and characterization of Cu-doped ZnO one-dimensional structures for miniaturized sensor applications with faster response. *Sens. Actuators A Phys.* **2013**, *189*, 399–408. [CrossRef]
64. Xiang, Z.; Gao, W.; Chen, L.; Lan, W.; Zhu, J.; Runge, T.M. A comparison of cellulose nanofibrils produced from Cladophora glomerata algae and bleached eucalyptus pulp. *Cellulose* **2015**, *23*, 493–503. [CrossRef]
65. Chen, M.; Kang, H.; Gong, Y.; Guo, J.; Zhang, H.; Liu, R. Bacterial Cellulose Supported Gold Nanoparticles with Excellent Catalytic Properties. *ACS Appl. Mater. Interfaces* **2015**, *7*, 21717–21726. [CrossRef] [PubMed]
66. Huang, Y.; Hang, T.; Hu, A.; Chen, Z.; Lu, Q.; Li, M. Solid state diffusion between Sn and Cu microcones on Cu microcones. *J. Alloys Compd.* **2014**, *582*, 408–413. [CrossRef]
67. Srivastava, A.; Kumar, N.; Khare, S. Enhancement in UV emission and band gap by Fe doping in ZnO thin films. *Opto-Electr. Rev.* **2014**, *22*, 68–76. [CrossRef]